Journal of Applied Electrochemistry (2005) 35:1127–1132
DOI 10.1007/s10800-005-9008-8

Selective etching of CoFeNiCu/Cu multilayers

Q. HUANG and E.J. PODLAHA*,[1]
Gordon A. and Mary Cain Department of Chemical Engineering, Louisiana State University, Baton Rouge, LA, 70803, USA
*(*author for correspondence, e-mail: podlaha@lsu.edu)*

Received 28 July 2004; accepted in revised form 21 June 2005

Key words: CoFeNiCu, corrosion, electrodeposition, multilayers

Abstract

Selective etching of CoFeNiCu/Cu multilayers was investigated with different solutions: HNO_3/alcohol, $FeCl_3$/HCl, $K_2Cr_2O_7/H_2SO_4$ and dilutions of $FeCl_3$/HCl, $K_2Cr_2O_7/H_2SO_4$. Polarization curves on a rotating disk electrode were used to assess the corrosion potential and current density of Cu, and Co-rich alloys. Preferential etching of the Co-rich alloy was attributed to either a less positive corrosion potential or a higher corrosion current density compared to the Cu layer. A dilution of the aqueous $K_2Cr_2O_7/H_2SO_4$ solution was considered most promising for submicron structure development.

1. Introduction

Compression molding has been widely used to produce features with sizes larger than 1 μm, such as in compact disks. Recently nanoimprinting has been demonstrated to expand the molding technique for the fabrication of nanostructures [1–3]. The advantage of imprint lithography lies in the cost-efficiency and high throughput. Studies have shown the applicability of the imprinting process for fabrication of features with dimension in the 10 nm scale with electron beam lithography [4–7]. Electrochemical methods, including electrodeposition and selective chemical etching, can be another alternative to prepare a nanometric mold without reliance on a lithographic step.

The electrodeposition of nanometric, compositionally modulated multilayers has been widely demonstrated, motivated by the interest in giant magnetoresistance (GMR) [8–14]. Due to the different composition of the alternating layers, it is possible to preferentially etch one layer with the other intact. In addition, selective etching of multilayered structures has been demonstrated in micron size layers in the development of microdevices [15, 16], and submicron size layers for improving SEM imaging contrast [17, 18]. Leith and Schwartz [15] developed a microgear from a lithographically fabricated layer structure of iron-rich and nickel-rich NiFe alloys. The less noble iron-rich layer was selectively etched in an acetic acid solution and the layer size was about 3 μm. In addition, Arai et al. [16] selectively etched Ni from a Ni/Cu system, by potentiostatic control in sulfuric acid. Bonhôte et al. [17] used a $K_2Cr_2O_7/H_2SO_4$ solution to selectively etch the more noble Cu layer in Ni/Cu multilayers for the examination of the multilayer structure with SEM, having layer sizes on the order of 10 nm. Similarly, a nitric acid–alcohol solution was used for etching Cu by Bradley and Landolt [18] for the Co/Cu system. This solution was also recently used in our group in the selective etching of Cu in the Ni/Cu and NiFe/Cu systems for developing grating structures for molding. [19] The selective etching of the more noble Cu layer compared to the less noble Ni, Co or NiFe is associated with the passivation of the less noble layer. Compared with the Ni/Cu and NiFe/Cu structures studied previously, the employment of the ternary alloy of Fe, Co and Ni will allow more flexibility in varying the deposit properties and controlling the etching selectivity through changes in the deposit composition.

In multilayers of alloys, selectivity of the etching solution is dependent upon the composition. Therefore, in this study, different etching solutions were characterized to determine appropriate conditions for the selective etching of CoFeNiCu/Cu nanometric multilayers, as a potential tool for fabrication of nanoimprinting molds. Deposition conditions of the alloys were characterized in previous studies [20–22]. Here, the etching conditions are characterized.

[1]ISE member.

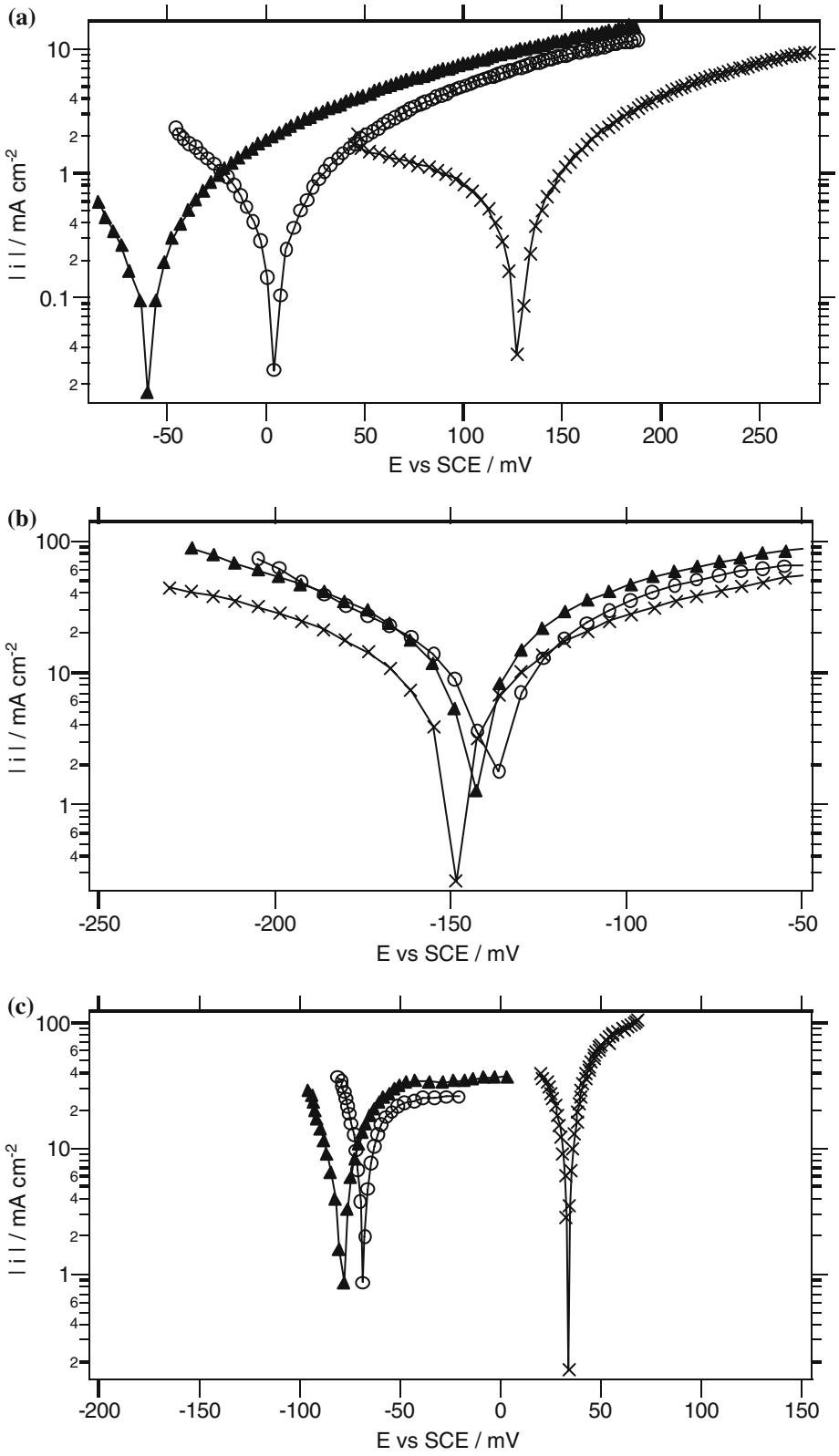

Fig. 1. Polarization curves of Cu (×) and alloy thin films deposited at −35.4 mA cm^{-2} (○), and −70.7 mA cm^{-2} (▲) in (a) HNO_3/alcohol solution; (b) $FeCl_3$/HCl solution; and (c) $K_2Cr_2O_7/H_2SO_4$ solution.

2. Experimental

A sulfate electrolyte with additives was used for electrodeposition of alloy thin films and multilayers, containing 8 mM $FeSO_4$, 50 mM $CoSO_4$, 57 mM $NiSO_4$, 1 mM $CuSO_4$, 27 mM sodium potassium tartrate, 10 mM sulfamic acid, 4 mM sodium saccharin and 0.6 g/l Triton X-100. Deposition was carried out on a gold-covered stainless steel rotating disk electrode (RDE), at 1000 rpm. Two DC-plated alloy deposits were used as

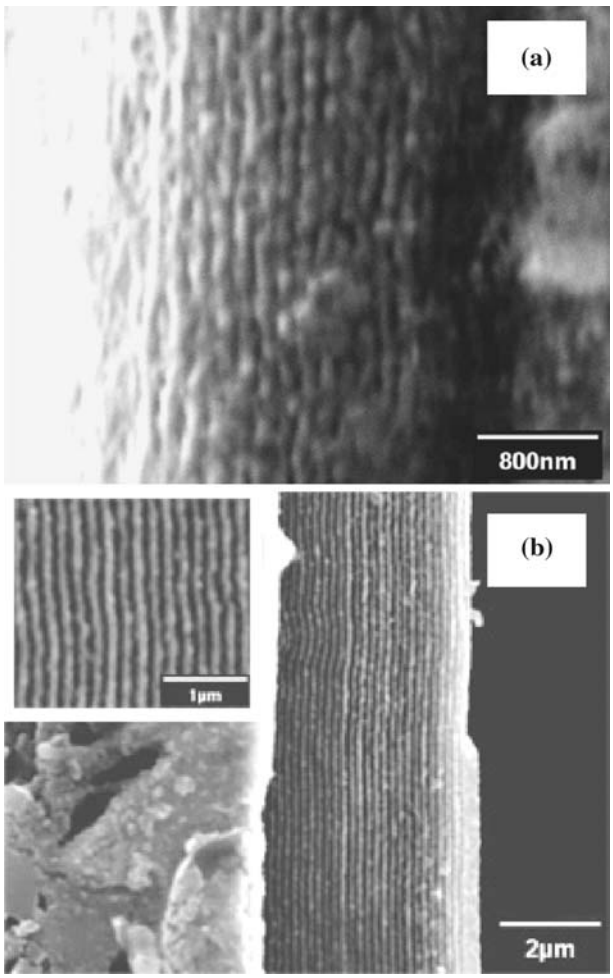

Fig. 2. SEM micrographs of a multilayer having sizes before etching of 130 nm of the Co-rich layer and 100 nm the Cu layer; (a) HNO_3/alcohol for 9 min (b) and $FeCl_3$/HCl solutions for 50 s. The insert in (b) is an enlargement.

substrates in this study: $Fe_{15}Co_{73}Ni_5Cu_7$ deposited at –35.4 mA cm^{-2}; and $Fe_{13}Co_{71}Ni_{13}Cu_3$ deposited at –70.7 mA cm^{-2}. For fast etching conditions in the $FeCl_3$/HCl and $K_2Cr_2O_7/H_2SO_4$ solutions, bulk, polycrystalline Cu was used (rods purchased from Goodfellow Corp.). For slow etching conditions found in the HNO_3/alcohol solution, Cu was plated as a thin film at -3.54 mA cm^{-2}.

Anodic polarization curves were measured on the RDE at 2000 rpm, with a PC-controlled Pine potentiostat and the potential was corrected for the ohmic drop, which is measured by impedance analysis with a BAS–Zahner IM6 impedance measurement unit. Multilayers were pulse plated with an Amel potentiostat together

Table 1. Corrosion current densities, i_{corr} (mA cm^{-2}), for different substrates in etching solutions

Substrates	Cu	$Fe_{15}Co_{73}Ni_5Cu_7$	$Fe_{13}Co_{71}Ni_{13}Cu_3$
HNO_3/alcohol	0.6	0.5	0.6
$FeCl_3$/HCl	10	11	28
$K_2Cr_2O_7/H_2SO_4$	50	10	10

Table 2. Corrosion potentials, E_{corr} (mV vs. SCE) for different substrates in etching solutions

Substrates	Cu	$Fe_{15}Co_{73}Ni_5Cu_7$	$Fe_{13}Co_{71}Ni_{13}Cu_3$
HNO_3/alcohol	125	4	−62
$FeCl_3$/HCl	−148	−138	−143
$K_2Cr_2O_7/H_2SO_4$	30	−68	−80

with a Waveteck function generator. Microstructures developed after etching were examined with a JEOL JSM-840A scanning electron microscope (SEM), operated at 20 kV. SEM preparation includes cross-sectional cutting, epoxy resin mounting, grounding and polishing, followed by selective etching of the sample. A 20-nm layer of gold was sputtered before imaging.

Three etching strategies were examined in this study, based on literature reports for the selective etching of Cu. The first one follows the study of Bradley and Landolt [18]. The polished cross-sectional sample was etched for 10 s in a dilute $K_2Cr_2O_7/H_2SO_4$ solution containing 0.036 M H_2SO_4, 0.0034 M $K_2Cr_2O_7$, and 0.0012 M HCl, followed by a nitric acid–alcohol solution, which is prepared by mixing 65% HNO_3 with ethanol by volumetric ratio 1:20. The action of the dilute $K_2Cr_2O_7/H_2SO_4$ was reported to etch both layers uniformly to expose the sample. The HNO_3/alcohol solution was responsible for the selective etching of Cu. The second solution was a $K_2Cr_2O_7/H_2SO_4$ solution, used by Bonhôte et al. [17] to selectively etch Cu in Ni/Cu multilayers. The solution contained 0.034 M $K_2Cr_2O_7$, 0.36 M H_2SO_4, and 0.012 M HCl. The third solution was an acidic ferric chloride–hydrochloric acid solution prepared by mixing 10 g $FeCl_3$, 25 ml HCl (36 wt%) and 100 ml H_2O. This solution was adapted from Pace Technologies [23] for etching Cu and Cu alloys. Apart from the first solution, etching in the latter two solutions is a one-step process.

3. Results and discussion

Figure 1 shows polarization curves of the different substrates in the three etching solutions. All the polarization curves follow Butler–Volmer behavior, with an anodic component due to substrate dissolution and a cathodic component arising from the electrolyte (H^+ and O_2) reduction. Linear extrapolation was used to obtain the corrosion potentials and current densities, which are presented in Tables 1 and 2. In the HNO_3/alcohol solution, Figure 1(a), the corrosion current densities of the three substrates are comparable. However, there is a large difference in corrosion potential. The more Cu in the deposit, the more noble is the corrosion potential. Therefore, the less noble Co-alloy will be prone to corrosion. In contrast, the corrosion potentials in the $FeCl_3$/HCl solution, Figure 1(b), are similar for the two different alloys and Cu, while the corrosion current densities differ significantly. In this case, all the alloys corrode but at different rates. For the

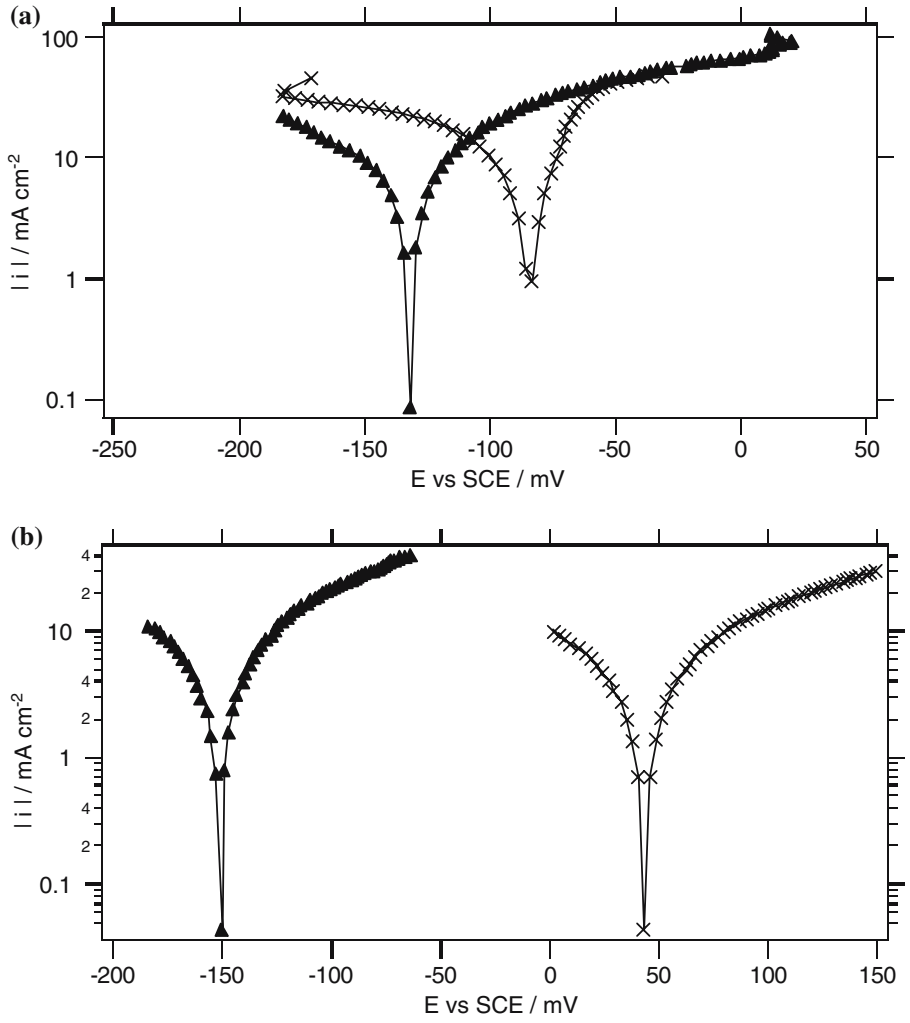

Fig. 3. Polarization curves of bulk polycrystalline Cu (×) and alloy thin films deposited at −70.7 mA cm^{-2} (▲) in (a) $FeCl_3$/HCl and (b) $K_2Cr_2O_7/H_2SO_4$ in a 1/4 dilution solution.

$K_2Cr_2O_7/H_2SO_4$ solution, Figure 1(c), the Cu has a more positive corrosion potential but a higher corrosion current density than the Co-rich alloys, so that this solution would provide the least selective etching.

The Co-rich alloy layer was etched in all three solutions without polarization, despite the fact that these solutions are mostly used for the selective etching of Cu in Ni/Cu and Co/Cu systems [17, 18]. This observation is believed to be ascribed to the presence of Fe in the Co-rich alloy, which renders the alloy less corrosion resistant. In addition, the presence of saccharin in the plating electrolyte introduces sulfur into the Co-rich layer, which was found [16, 24] to deteriorate the corrosion resistance and thus alter the etching selectivity. In HNO_3/alcohol solutions, the relatively negative corrosion potential for the Co-rich alloys make it prone to attack, while in the $FeCl_3$/HCl solution, the higher corrosion current density of the Co-rich alloys favors etching.

Table 3. Corrosion current densities, i_{corr}, and corrosion potentials, E_{corr} (vs. SCE) for the Cu and Co-rich alloy in dilute solutions

	Cu		$Fe_{13}Co_{71}Ni_{13}Cu_3$	
	i_{corr}/mA cm^{-2}	E_{corr}/mV	i_{corr}/mA cm^{-2}	E_{corr}/mV
Diluted $FeCl_3$/HCl	15	−83	7	−132
Diluted $K_2Cr_2O_7/H_2SO_4$	5	43	9	−150

For the two selective electrolytes, a multilayer structure was developed from the plating bath and etched (Figure 2). The multilayers were pulse plated between −70.7 mA cm^{-2} for 15.2 s and −3.54 mA cm^{-2} for 131.9 s. Calculation of the layer sizes with reported current efficiencies in ref. [20] results in a Co-rich layer of 130 nm and a Cu layer of 100 nm. Figure 2 shows the grating structures etched from multilayers and sputtered with Au for SEM imaging. The depth profile was not measured, but is proportional to the etching time. Etching was carried out in the HNO_3/alcohol solution for 9 min, Figure 2(a), which was not sufficient to fully develop the nanostructures. In comparison, a multilayer structure with the same layer thicknesses was etched in the $FeCl_3$/HCl solution for 50 s, shown in Figure 2(b). Due to the larger corrosion current density, Table 1, a

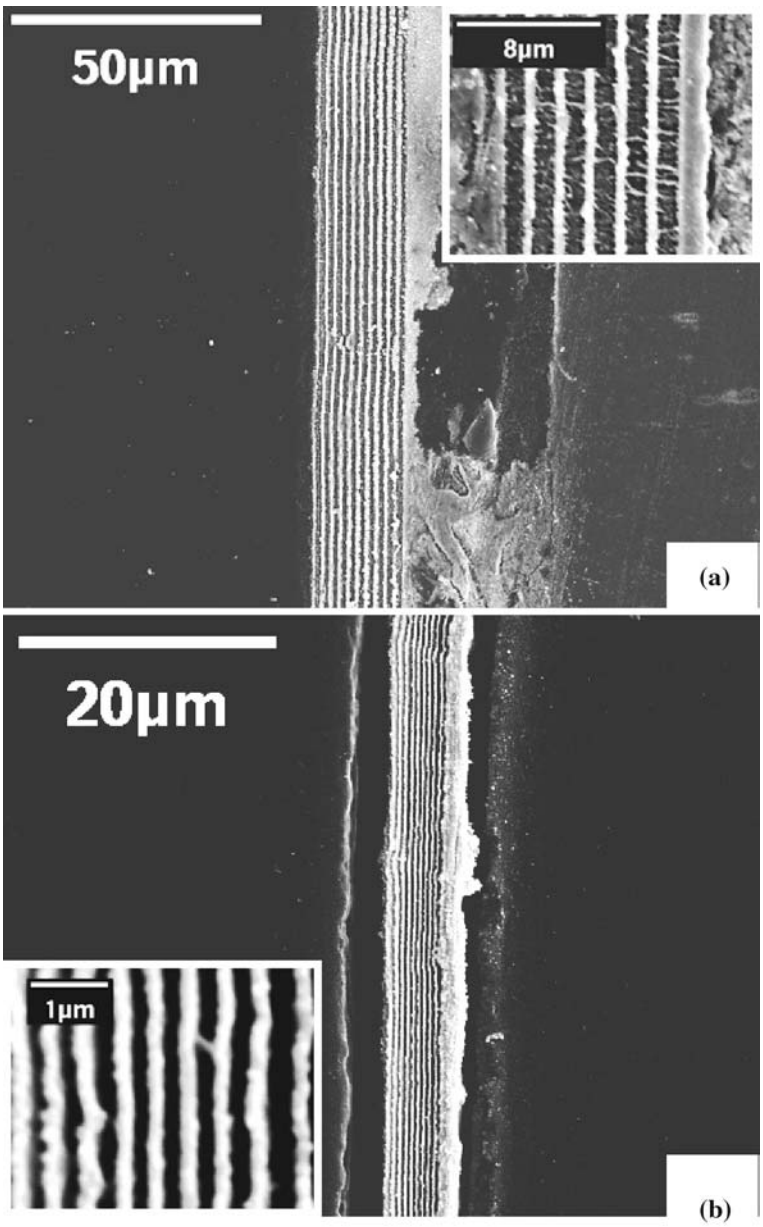

Fig. 4. SEM micrographs of the multilayers after etching with four-fold volumetrically diluted $K_2Cr_2O_7/H_2SO_4$ solution: (a) 1000 nm Co-rich alloy and 500 nm Cu, etched for 2 min and (b) 200 nm Co-rich alloy and Cu layers etched for 3 min.

shorter etching time is needed for the $FeCl_3$/HCl solution compared to the HNO_3/alcohol. Waviness in the multilayers was observed for the structures in Figure 2(b), which is believed to result from the grain growth in the multilayer deposition. Similar results have been reported by Bonhote et al. [17] and Lim et al. [19]. The high etching rate of $FeCl_3$/HCl is believed to further increase the non-uniformity of the layer width accentuating the waviness.

In order to further improve selectivity, polarization studies were carried out in a 1/4 diluted $FeCl_3$/HCl and $K_2Cr_2O_7/H_2SO_4$ solutions. No dilution of the HNO_3/alcohol solution was considered since it would further lower an already low dissolution rate. A comparison between the four-fold volumetrically diluted solution is shown in Figure 3 for the (a) $FeCl_3$/HCl and (b) $K_2Cr_2O_7/H_2SO_4$ solutions. The corresponding corrosion potentials and current densities are listed in Table 3. In the $FeCl_3$/HCl solutions, either concentrated or diluted, Cu is always more corrosion resistant than the Co-rich alloy. The difference of the corrosion potential is significantly larger in the diluted solution. However the Cu corrosion current density becomes higher than the Co-rich alloy in the diluted solution, which favors the etching of Cu and thus makes the selectivity deteriorate. In the four-fold diluted $K_2Cr_2O_7/H_2SO_4$ solutions, the difference of the corrosion potential for the two layers was also increased compared with the concentrated solution, favoring the Co-rich layer etching. Furthermore, the corrosion rates were decreased more for Cu than the Co-rich alloy. Therefore, the Co-rich alloy corrosion is more selective compared to

Cu with the effects from corrosion potentials and corrosion current density reinforcing each other.

Figures 4(a) and (b) show the SEM images of two different multilayers after selective etching with the four-fold volumetrically diluted $K_2Cr_2O_7/H_2SO_4$ solution. Some residue was observed in the etched layer. However, the improvement regarding the structure quality using the dilute $K_2Cr_2O_7/H_2SO_4$ etchant is evident. The multilayers were plated with same pulse plating scheme as in Figure 2 (-3.54 mA cm^{-2} and -70.7 mA cm^{-2}) with a change in deposition times. The larger layer thicknesses were plated for 121 and 657 s for the Co-alloy and Cu layers, respectively, Figure 4(a). Following etching, the layer sizes were 1000 nm of the Co-rich alloy layer and 500 nm of the Cu layer, consistent with the calculated values. Thinner layers were pulsed plated at 24 and 263 s for the Co-alloy and Cu layer and the layer size were also consistent with the plated layer size of 200 nm. The high quality etch evident in the SEM micrographs required a longer etching time compared to the $FeCl_3$/HCl solution, consistent with the lower corrosion current densities (compare Tables 1 and 3). The dilute $K_2Cr_2O_7/H_2SO_4$ solution is similar in its selectivity as the HNO_3/alcohol solution in that there is a large difference in the corrosion potential between the Co-rich alloy and Cu. The advantage of the dilute $K_2Cr_2O_7/H_2SO_4$ solution is that the dissolution rate of the metals is larger than that of the HNO_3/alcohol solution. In addition the avoidance of the organic solvent has an advantage for samples mounted in plastic resins, which is typically carried out for SEM analyses.

4. Conclusions

Evaluation of etching solutions for CoFeNiCu/Cu multilayers showed that Co-rich alloys are preferentially etched in the HNO_3/alcohol, $FeCl_3$/HCl and dilute $K_2Cr_2O_7/H_2SO_4$ solutions. The selective etching of the Co-rich alloy over Cu was attributed to the less positive corrosion potential in HNO_3/alcohol and $K_2Cr_2O_7/H_2SO_4$ solutions, while in the $FeCl_3$/HCl case the higher corrosion current density was responsible for the selective etching. The dilution of the $K_2Cr_2O_7/H_2SO_4$ solutions was found to improve the selectivity of Co-rich alloy over Cu.

Acknowledgements

This work was supported by the National Science Foundation.

References

1. S.Y. Chou, P.R. Krauss and P.J. Renstrom, *Science* **272** (1996) 85.
2. S.Y. Chou, P.R. Krauss and P.J. Renstrom, *J. Vacuum Sci. Technol. B* **14** (1996) 4129.
3. C.M. Sotomayor Torres, S. Zankovych, J. Seekamp, A.P. Kam, C. Clavijo Cedeno, T. Hoffmann, J. Ahopelto, F. Reuther, K. Pfeiffer, G. Bleidiessel, G. Gruetzner, M.V. Maximov and B. Heidari, *Mater. Sci. Eng. C: Biomimetic Supramol. Sys.* **C 23** (2003) 23.
4. S.Y. Chou, P.R. Krauss and P.J. Renstrom, *Appl. Phys. Letts* **67** (1995) 3114.
5. S.Y. Chou, P.R. Krauss, W. Zhang, L. Guo and L. Zhuang, *J. Vacuum Sci. Technol. B* **15** (1997) 2897.
6. M. Li, J. Wang, L. Zhuang and S.Y. Chou, *Appl. Phys. Letts* **76** (2000) 673.
7. J. Wang, S. Schablitsky, Z. Yu, W. Wu and S.Y. Chou, *J. Vac. Sci. Technol. B* **17** (1999) 2957.
8. M.N. Baibich, J.M. Broto, A. Fert, F. Nguyen Van Dau, F. Petroff, P. Eitenne, G. Creuzet, A. Friederich and J. Chazelas, *Phys. Rev. Letts.* **61** (1988) 2472.
9. G. Binasch, P. Gruenberg, F. Saurenbach and W. Zinn, *Phys. Rev. B Condense Matter Mater. Phys.* **39** (1989) 4828.
10. M. Jimbo, T. Kanda, S. Goto, S. Tsunashima and S. Uchiyama, *J. Appl. Phys.* **31**(part 2) (1992) L1348.
11. M. Alper, K. Attenborough, R. Hart, S.J. Lane, D.S. Lashmore, C. Younes and W. Schwarzacher, *Appl. Phys. Letts* **63** (1993) 2144.
12. C.A. Ross, *Annu. Rev. Mater. Sci.* **24** (1994) 159.
13. K.D. Bird and M. Schlesinger, *J. Electrochem. Soc.* **142** (1995) L65.
14. E. Chassaing, P. Nallet and M.F. Trichet, *J. Electrochem. Soc.* **143** (1996) L98.
15. S.D. Leith and D.T. Schwartz, *J. Micromech. Microeng.* **9** (1999) 97.
16. S. Arai, T. Hasegawa and N. Kaneko, *J. Electrochem. Soc.* **150** (2003) C798.
17. C. Bonhote and D. Landolt, *Electrochim. Acta* **42** (1997) 2407.
18. P.E. Bradley and D. Landolt, *Electrochim. Acta* **45** (1999) 1077.
19. Lim Che-Yih, Q. Huang, X. Xie, A. Safir, S.A. Harfenist, R. Cohn and E.J. Podlaha, *J. Appl. Electrochem.* **34** (2004) 857.
20. Q. Huang, D.P. Young, J.Y. Chan, J. Jiang and E.J. Podlaha, *J. Electrochem. Soc.* **149** (2002) C349.
21. Q. Huang, D.P. Young and E.J. Podlaha, *J. Appl. Phys.* **94** (2003) 1864.
22. Q. Huang and E.J. Podlaha, *J. Electrochem. Soc.* **151** (2004) C119.
23. http://www.metallographic.com/4Technical.htm.
24. T. Osaka, M. Takai, Y. Sogawa, T. Momma, K. Ohashi, M. Saito and K. Yamada, *J. Electrochem. Soc.* **146** (2004) 2092.